Desalination and Water Treatment
www.deswater.com

doi: 10.5004/dwt.2021.26679

213 (2021) 26–34
February

Modeling and simulation of water production for different solar still heights and condensation surfaces

Hiba Akrout*, Khaoula Hidouri, Béchir Chaouachi, Romdhane Ben Slama

Research Laboratory Energy, Water, Environment and Process, National Engineering School of Gabes, Omar Ibn El Khattab Avenue, Gabes 6029, Tunisia, emails: akrouthiba@gmail.com (H. Akrout), khaoula2013@yahoo.fr (K. Hidouri), bechir.chaouachi@enig.rnu.tn (B. Chaouachi), romdhaneb.slama@gmail.com (R. Ben Slama)

Received 1 November 2019; Accepted 9 October 2020

ABSTRACT

This paper presents the modeling of single-slope solar still for water desalination based on a system of heat and mass balances. To evaluate the solar still performance, it is important to accurately quantify heat and mass transfer phenomena inside the solar still. Heat and mass correlations used in this model include the distance between evaporation and condensation surfaces as a variable parameter that affects production. Results show that increasing the solar still height by 20 cm, for constant water depth and inclination angle, reduces its production by 168 mL. Besides, the suggested theoretical model focuses on the importance of choosing the condensation surface material and its effect on distiller performance. The solar radiation transmittance through water droplets fixed on the condensation surface depends on the contact angle that the droplets form with the condensation surface. Results show that the production for glass is almost twice higher than that for plexiglass or polycarbonate. Moreover, the effect of other parameters, such as water depth, insulation thickness, and different insulation materials, on distiller performance was studied. The proposed model has been approved as there is a good agreement between the theoretical results and the experimental measurements.

Keywords: Solar still; Heat and mass transfer; Distiller height; Contact angle; Droplets transmittance

1. Introduction

Currently, many regions in the world encounter water supply difficulties that are due to the depletion of freshwater resources, enormous population growth, and industrial development. As the sea covers more than 70% of the earth's surface, seawater desalination is considered as an efficient solution to satisfy freshwater needs. Reverse osmosis and distillation, specifically multi-stage-flash (MSF) distillation and multi-effect distillation (MED), are widely used for areas with huge water demand. However, these technologies have a large energy consumption, especially for MSF and MED. Simple solar distillation is one of the low-cost, simple, and clean technologies of desalination. Considering its low productivity, simple solar still may be useful in remote areas with low population density and abundant solar energy for domestic use or agriculture.

The solar distillation process consists of heating and evaporating the water by solar radiation that is transmitted through the transparent cover to the saline water contained in the basin. The basin is coated with high solar absorbent material for more efficiency. The water vapor condensation then occurs on the inner part of the condensation surface and, thus, distillate water is recovered.

* Corresponding author.

Over the years, scientists have studied the different configurations of solar stills. The water production of the simple solar distillation with the greenhouse effect is low. Hence the interest of several theoretical and experimental works was in improving its performance. For example, adding copper oxide and graphite micro-flakes to the brine basin increases the solar still productivity by 44.91% and 53.95%, respectively. Furthermore, cooling the glass with feed water increases the distillate rate by 47.8% and 57.6% using the copper oxide and graphite micro-flakes, respectively [1]. Besides, it has been reported that a solar distiller integrated with an external condenser and a fan provides a daily efficiency of 46.23%. The daily efficiency increases when using aluminum oxide and cuprous oxide nanoparticles and reaches 73.85% and 84.16%, respectively [2].

Moreover, adding a phase change material (PCM), which is a thermal storage material, to the base and sides of a simple solar still enhances its productivity. Using aluminum powder with PCM improves its thermal conductivity and then increases further distiller productivity [3]. A jute cloth knitted with sensible heat storage material incorporated in a simple solar still provides a higher production than that without jute cloth, that is, 5.9 kg/m^2 compared with 5 kg/m^2 [4].

The glass cover thickness also affects production as it has been demonstrated that reducing the glass cover thickness increases heat and mass transfer inside the solar still and consequently production [5]. A multi-effect solar still with corrugated condensation surfaces decreases the condensation resistance, thus increasing production [6].

By experimentally testing different shapes of trays for a multi-stage solar still, it has been concluded that the V shape trays are the most efficient ones for distillate water production [7]. It has been reported that the efficiency of the solar still with the compression heat pump is 75% higher than that of simple solar still [8]. Besides, a hybrid solar still integrated with an air compressor gives higher performance than that without an air compressor [9]. Experiments have also reported that the productivity of a solar still coupled to flat plate collector is about 10.061 L/m^2 d, and its internal thermal efficiency is equal to 80.6% while the passive solar still productivity is equal to 7.8 L/m^2 d and its internal efficiency is about 57.1% [10].

Furthermore, many researchers have focused on the convection and mass transfer mechanisms that occur in the simple solar still to evaluate its performance. Dunkle correlations have first been proposed to estimate convection and mass transfer [11]. These correlations are available for a mean humid air temperature of 50°C and a temperature difference of 17°C. Another assumption for the Dunkle model is that the effect of distance variation between hot and cold surfaces on production is neglected. Dunkle model has been widely used and accepted by many researchers working in the solar distillation area. However, other correlations from the literature estimate free convection and consider the distance between hot and cold surfaces as a variable that affects the convection transfer. These correlations represent a relation between the Nusselt number, the Grashof number, and the Prandtl number [12]. A modified Grashof number was presented to evaluate the convection accompanied by evaporation in the solar still [13]. Also, it has been found that the mass rate calculated by Lewis correlation agrees well with the experimental results for both simple solar still and solar still coupled to a compression heat pump [14]. Another study has demonstrated that the theoretical production of the Kumar and Tiwari model is close to the experimental production of a conventional solar still, the variation is almost equal to 12.31%. However, the Clark model overpredicts the experimental production by 82.4% [15]. Moreover, it has been revealed that using a porous absorber with fine black stones instead of the simple absorber used in conventional solar still increases the average Nusselt and Sherwood numbers by 115.00% and 51.95%, respectively [16].

The main purpose of the present work is to simulate the solar still performance for different heights, different condensation surfaces, and other parameters affecting the still productivity, namely water depth and insulation type and thickness.

The effect of specific height variation on solar still performance has already been studied experimentally in the literature. A correlation for Nusselt number estimation as a function of specific height has been developed based on experimental results. Another correlation between daily efficiency and specific height has also been established. The distiller specific height reduction has been proven to increase daily efficiency [17]. This paper also presents a theoretical investigation on the effect of distance (x) variation on simple solar still performance. The proposed heat and mass transfer correlations enable us to accurately evaluate the distiller performance for different heights of the solar still. Besides, the proposed model presents the sides losses variation as a function of solar still height and its effect on performance.

Moreover, it has been shown experimentally in the literature that a plastic solar still with a glass cover for a water depth of 10 cm is 30%–35% more productive than that with similar geometric features but with a plexiglass cover [18]. Experiments conducted for different transparent materials, such as polyethylene terephthalate and glass, show that materials with low contact angle, such as glass, allow more sunlight transmittance through water droplets and ensure the best production [19]. The main conclusion is that the material contact angle is the primordial parameter that affects the solar still performance. The proposed model predicts the theoretical production of the solar still for different condensation surfaces based on the solar irradiation transmittance. Solar irradiation transmittance through water droplets, which depends on the contact angle of the condensation surface, is a variable parameter in this model.

2. Solar still description

The solar still basin is coated with a 0.7 mm thick galvanized iron sheet painted in black. The saline water is heated and then evaporated thanks to the sunlight's thermal energy transmitted through a 3 mm thick plexiglass cover and then absorbed by the basin. The water vapor is then condensed on the transparent cover, and the distillate water is collected. The distiller sides are coated with mirror sheets to re-reflect the rays. The heat losses from the distiller bottom and sides to the outside atmosphere are reduced by glass wool of 2.5 cm thickness. A scheme of the solar still is given in Fig. 1. The still dimensions and material properties are presented in Table 1. The reflectivity of water inside the solar still is neglected.

Table 1
Properties and dimensions of different components of the solar still

	Plexiglass	Basin/absorber	Water in basin
Area (m^2)	0.94	0.84	0.84
Specific heat (J/kg°C)	1,462	462	4,090
Transmissivity	0.91	–	0.95
Absorptivity	0.04	0.95	0.05
Reflectivity	0.05	0.05	0.0
Thermal conductivity (W/m K)	–	73	0.6
Length (m)	1	1	1
Width (m)	0.93	0.84	0.84

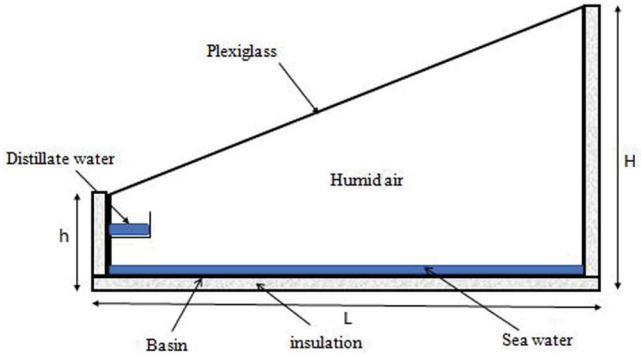

Fig. 1. Descriptive schema of single-slope solar still.

3. Theoretical model

The developed theoretical model is based on energy and mass balances for different components of solar still to simulate its performance. The model assumptions are as follows:

- The temperature gradients along the plexiglass thickness and water depth are negligible.
- The water depth is kept constant.
- The solar still is vapor proof.
- The plexiglass has an optimal inclination.
- Water droplets transmittance values are based on normally incident light.

Energy balances for the plexiglass, water, and basin are given below:

The plexiglass energy balance is given as follows:

$$\frac{m_{pg}C_{ppg}}{S_{pg}}\frac{dT_{pg}}{dt}=\alpha_{pg}G+\left(q_{ew}+q_{c,w-pg}+q_{r,w-pg}\right)-q_{r,pg-a}-q_{c,pg-a} \quad (1)$$

The water energy balance is given as follows:

$$\frac{m_w C_{pw}}{S_w}\frac{dT_w}{dt}=\tau_{pg}\tau_{dr}\alpha_w G+q_{c,b-w}-\left(q_{ew}+q_{c,w-pg}+q_{r,w-pg}\right) \quad (2)$$

The absorber energy balance is given as follows:

$$\frac{m_b C_{pb}}{S_b}\frac{dT_b}{dt}=\tau_{pg}\tau_{dr}\tau_w\alpha_b G-q_{c,b-w}-q_{losses(b)} \quad (3)$$

The distillate rate is obtained based on the analogy of heat and mass transfer of boundary layers [20] as follows:

$$\dot{m}=h_m\frac{M_w}{R}\left(\frac{P_w}{T_w}-\frac{P_{pg}}{T_{pg}}\right) \quad (4)$$

where the convective mass transfer coefficient is given as follows:

$$h_m=\frac{h_{c,w-g}}{\rho_{ha}C_{pha}Le^{(1-n)}} \quad (5)$$

with $n=\frac{1}{4}$ if $2.8\times10^3<Gr<2.1\times10^5$

$n=\frac{1}{3}$ if $4.2\times10^5<Gr<4.2\times10^9$

The different heat transfers presented above may be divided into two groups: external heat transfer and internal heat transfer.

3.1. Internal heat transfer

The convective heat transfer from water to plexiglass is determined through the estimation of the Nusselt number as follows:

$$q_{c,w-pg}=h_{c,w-pg}\left(T_w-T_{pg}\right) \quad (6)$$

Jakob and Gupta evaluated the Nusselt number in their experiments as follows [12]:

$$Nu=0.3\left(Gr\,Pr\right)^{1/4} \quad \text{if} \quad 2.8\times10^3<Gr<2.1\times10^5 \quad (7)$$

$$Nu=0.1255\left(Gr\,Pr\right)^{1/3} \quad \text{if} \quad 4.2\times10^5<Gr<4.2\times10^9 \quad (8)$$

The Nusselt expressions given above are applicable for free convection only. However, the convection in solar distiller is accompanied by mass transfer. For this reason, Sharpley and Boetler [13] proposed a modified Grashof number to estimate this kind of convection in the solar still.

The expression of the modified Grashof number is given as follows:

$$Gr_m=\frac{x^3\rho_{ha}{}^2\beta_{ha}g}{u_{ha}^2}\left[\left(T_w-T_{pg}\right)+\frac{\left(P_w-P_{pg}\right)\left(T_w+273.15\right)}{268.9\times10^3-P_w}\right] \quad (9)$$

where the convection coefficient from water to plexiglass is as follows:

$$h_{c,w-\mathrm{pg}} = \frac{\mathrm{Nu}K_{\mathrm{ha}}}{x} \tag{10}$$

The evaporation heat transfer from water to plexiglass is given as follows:

$$q_{\mathrm{ew}} = \dot{m}L_v \tag{11}$$

The convective heat transfer from basin to water is given by [21]:

$$q_{c,b-w} = h_{c,b-w}\left(T_b - T_w\right) \tag{12}$$

where the convective coefficient from basin to water is [22] as follows:

$$h_{c,b-w} = \frac{0.54\left(K_w \mathrm{Ra}_w^{\frac{1}{4}}\right)}{L_w} \quad \text{if} \quad 10^4 < \mathrm{Ra}_w < 10^7 \tag{13}$$

$$h_{c,b-w} = \frac{0.15\left(K_w \mathrm{Ra}_w^{\frac{1}{3}}\right)}{L_w} \quad \text{if} \quad 10^7 < \mathrm{Ra}_w < 10^{11} \tag{14}$$

The radiation heat flux from water to plexiglass is [23] as follows:

$$q_{r,w-\mathrm{pg}} = \varepsilon_{\mathrm{eff}}\sigma\left(T_w^4 - T_{\mathrm{pg}}^4\right) \tag{15}$$

where

$$\varepsilon_{\mathrm{eff}} = \frac{1}{\left(\frac{1}{\varepsilon_w} + \frac{1}{\varepsilon_{\mathrm{pg}}} - 1\right)} \tag{16}$$

3.2. External heat fluxes

The radiation heat transfer from plexiglass to the outside atmosphere is [23] as follows:

$$q_{r,\mathrm{pg}-a} = \varepsilon_{\mathrm{pg}}\sigma\left(T_{\mathrm{pg}}^4 - T_{\mathrm{sky}}^4\right) \tag{17}$$

where the sky temperature is given by equation as follows [24]:

$$T_{\mathrm{sky}} = T_a - 6 \tag{18}$$

The convective heat transfer from plexiglass to the distiller outside [25] is given as follows:

$$q_{c,\mathrm{pg}-a} = h_{c,\mathrm{pg}-a}\left(T_{\mathrm{pg}} - T_a\right) \tag{19}$$

Its coefficient is given as follows [26]:

$$h_{c,\mathrm{pg}-a} = 6.15 \times V_{\mathrm{wind}} \quad \text{if} \quad V_{\mathrm{wind}} > 5\mathrm{m/s} \tag{20}$$

$$h_{c,\mathrm{pg}-a} = 2.8 + 3 \times V_{\mathrm{wind}} \quad \text{if} \quad V_{\mathrm{wind}} < 5\mathrm{m/s} \tag{21}$$

The basin heat losses from bottom and sides to the distiller outside equation are given as follows [24]:

$$q_{\mathrm{losses}(b)} = U_b\left(T_b - T_a\right) \tag{22}$$

where the heat losses coefficient is obtained as follows [21,28]:

$$U_b = \left(\frac{L_b}{K_b} + \frac{L_i}{K_i} + \frac{1}{h_{c,b-a}}\right) + \frac{S_{\mathrm{ss}}}{S_b}\left(\frac{L_b}{K_b} + \frac{L_i}{K_i} + \frac{1}{h_{c,b-a}}\right) \tag{23}$$

Note: all the thermophysical properties are calculated at the humid air temperature, which is the average temperature between the water surface and the plexiglass cover, and are given as follows:

$$C_{\mathrm{pha}} = 0.9992 \times 10^3 + 1.4339 \times 10^{-1} T_{\mathrm{ha}} + 1.1010 \times 10^{-4} T_{\mathrm{ha}}^2 - 6.7581 \times 10^{-8} T_{\mathrm{ha}}^3 \tag{24}$$

$$K_{\mathrm{ha}} = 0.0244 + 0.7673 \times 10^{-4} T_{\mathrm{ha}} \tag{25}$$

$$\rho_{\mathrm{ha}} = \frac{353.44}{\left(T_{\mathrm{ha}} + 273.15\right)} \tag{26}$$

$$u_{\mathrm{ha}} = 1.718 \times 10^{-5} + 4.62 \times 10^{-8} T_{\mathrm{ha}} \tag{27}$$

$$\beta_{\mathrm{ha}} = \frac{1}{\left(T_{\mathrm{ha}} + 273.15\right)} \tag{28}$$

$$L_v = 2{,}324.6\left(\begin{matrix}1.0727 \times 10^3 - 1.0167 \times T_{\mathrm{ha}} + 1.4087 \times 10^{-4} T_{\mathrm{ha}}^2 \\ -5.1462 \times 10^{-6} T_{\mathrm{ha}}^3\end{matrix}\right) \tag{29}$$

where the temperature of humid air is given by $T_{\mathrm{ha}} = \frac{T_w + T_{\mathrm{pg}}}{2}$.

4. Numerical resolution

A numerical resolution of the energy and mass balances equation system given previously was carried out using MATLAB software. This computer simulation was conducted to determine the optimal operating conditions of the solar still. Many parameters affect the solar still performance, such as the solar distiller geometry, the type of component material, etc. Varying one parameter in this simulation program affects the solar still distillate rate. The fourth-order Runge–Kutta method was used for the heat and mass transfer equations resolution, which are first-order differential equations. The solar still components initial temperatures were assumed to be equal to ambient temperature. The time step for this simulation program is equal to 1 h. The temperatures of plexiglass, water, and basin, as well as the distillate rate, are determined each hour from 9:00 am to 6:00 pm.

5. Results and discussion

The experimental study was conducted in February and March at different ambient conditions. The ambient temperature was found to be around 13°C–26°C, while the wind speed was around 0–6 m/s. Fig. 2 presents the ambient temperature as well as the wind speed variation along the experimental days.

Fig. 3 illustrates the variation of solar intensity as a function of time from 7:00 am to 6:00 pm on 28 February, 13 and 14 March: Solar intensity increases gradually until a maximal value around 12:00 am and 1:00 pm, then decreases.

To validate our model, we made a comparison between theoretical and experimental results. Fig. 4 shows that the deviation between the proposed model results and experimental measurements is narrow. This deviation is due to the model assumptions detailed above. The average absolute relative error is almost equal to 10%.

As can be seen in Fig. 5, the temperatures of the distiller components follow a parabolic profile similar to that of the solar intensity in Fig. 3. Temperatures increase gradually until reaching maximal values between 1:00 pm and 2:00 pm then decrease. The maximum basin temperature is about 55°C, whereas it is about 40°C for the plexiglass. The high temperature of the basin is due to the high absorption coefficient of the galvanized iron sheet painted in black. The water temperature is slightly lower than that of the basin. This difference in temperature between water and plexiglass leads to freshwater production.

Fig. 6 illustrates the cumulative distillate rate of the solar still along the day. The production reaches 1,859 mL/m^2 at 6:00 pm. The hourly distillate rate produced increases gradually at the start of the day and reaches the highest value between 1:00 pm and 2:00 pm then decreases again.

The parametric study carried out shows how the variation of one parameter may affect the production. Varying the average distiller height for constant water depth means that the average distance (x) between evaporation and condensation surfaces is variable too.

Average distiller height is given by $H_m = \frac{H+h}{2}$

Table 2 shows the theoretical variation of the production with different heights of the solar still. Reducing the height for fixed basin surface, fixed angle of inclination, and constant water depth induce the augmentation of production. This may be explained by the relation between convective heat coefficient from water to plexiglass and the average distance between hot and cold surface (x) given in Eq. (10). The convective coefficient is inversely proportional to the average distance (x). Moreover, the decrease of average solar still height reduces the sides heat losses to the outside atmosphere because the sides area becomes smaller.

The light transmittance upon different fogged surfaces, such as glass, polyethylene, and polystyrene, has been studied theoretically and experimentally [28]. The study results prove that water droplets' geometry is the main parameter affecting the transmittance. The contact angle is the angle a water droplet creates with the condensation surface when deposited on it. The transmittance through water droplets is about 90% for contact angle equal to 0° and remains constant up to a contact angle of 40°, then declines significantly beyond this value. The lowest transmittance happens for a contact angle of 90° [28]. Since the sunlight transmittance affects the solar still production, the transparent cover material should have a contact angle equal to or less than 40° as glass.

Although glass ensures a high transmittance, it is a weighty and brittle material, while plastics such as

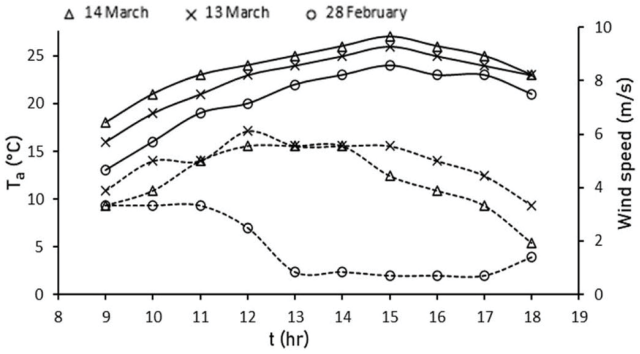

Fig. 2. Variation of ambient temperature and wind speed along experimental days (28 February, 13 and 14 March), the straight and dashed lines represent the ambient temperature and wind speed, respectively.

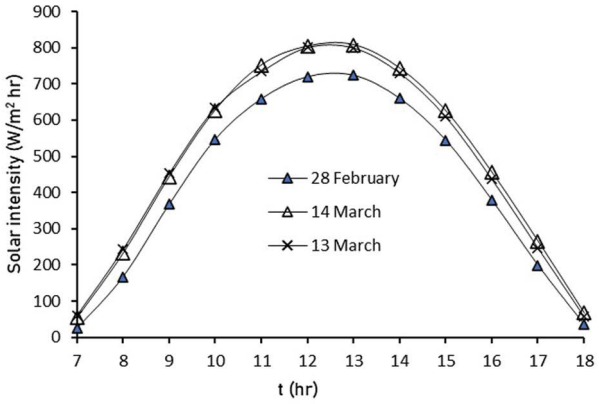

Fig. 3. Solar intensity vs. local time.

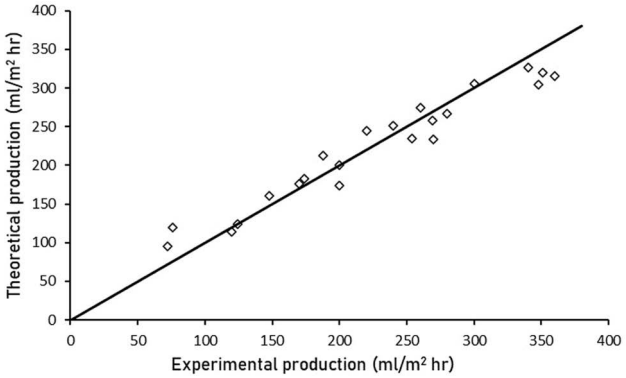

Fig. 4. Experimental validation of the mathematical model.

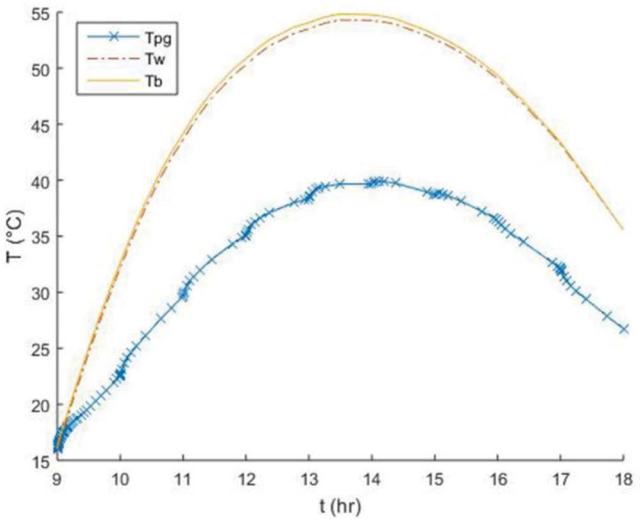

Fig. 5. Theoretical variation of plexiglass, water, and absorber temperatures along the day of 13 March.

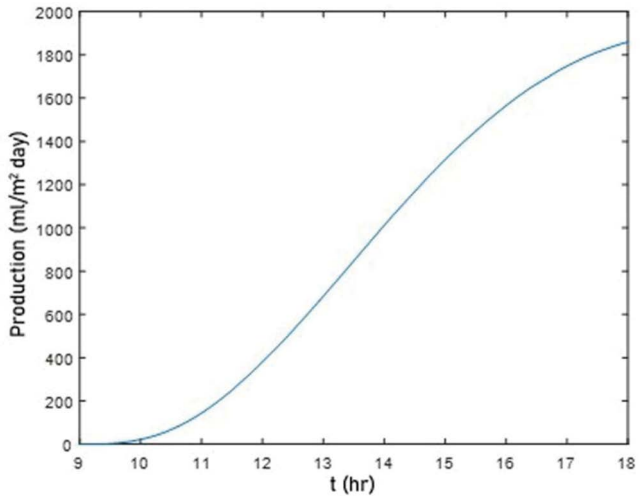

Fig. 6. Theoretical cumulative production of simple solar distiller on 13 March.

plexiglass, polyethylene, and polystyrene are light materials and less fragile [19]. However, the major inconvenience with plastics is the low transmittance due to their high contact angle. As a solution to this problem, the hydrophobic character of plastics can be reduced by modifying their surfaces [28]. Table 3 regroups different condensation surfaces, contact angles, and droplets transmittance. Fig. 7 presents the variation of solar still production with different condensation surfaces, such as glass, plexiglass, unclean glass, and polycarbonate. The solar still production is more important for surfaces with low contact angles.

Model results show that the maximal hourly production for glass, plexiglass, unclean glass, and polycarbonate is about 597, 327, 512, and 281 mL/m^2 h, respectively. Transmittance through water droplets τ_{dr} is a variable parameter that depends on the condensation surface used in solar still and is given in Eqs. (2) and (3).

Table 2
Variation of theoretical cumulative production with different solar still heights on March 13 (plexiglass cover)

H (cm)	*h* (cm)	Inclination	*V* (mL/d)
0.49	0.10	25	2,035
0.59	0.20	25	1,949
0.69	0.30	25	1,867

Table 3
Contact angle and droplets transmittance for different condensation surfaces [27]

	Contact angle	Droplets transmittance τ_{dr}
Glass	0°	91%
Plexiglass	71°	58%
Unclean glass	96°	81%
Polycarbonate	82°	52%

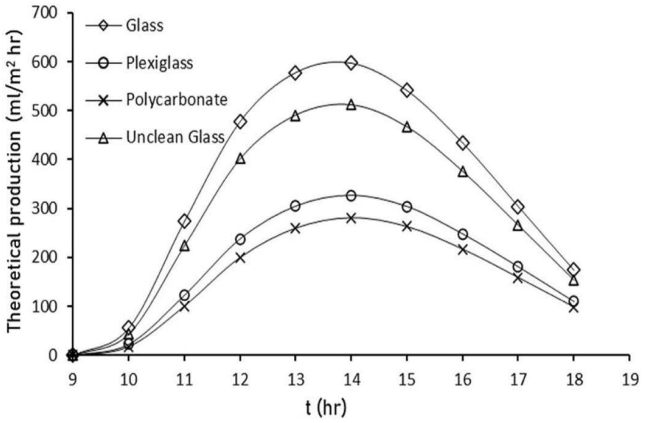

Fig. 7. Effect of condensation surface on the solar still production on 13 March.

Fig. 8 illustrates the variation of daily cumulative production and saline water temperature as a function of water depth. Although the increase in the water depth reduces the average distance (*x*) between hot and cold surfaces, the total production is reduced. This may be explained by the fact that the production increases due to the diminution of distance (*x*) (Table 2) is very low compared with its decrease due to the rise in water mass. As can be seen in Fig. 6, the increase of water mass or depth under the same solar intensity from 2 to 4 cm reduces the basin water temperature by 8°C at 1:00 pm, then the water vapor pressure decreases, which causes the reduction of total production by 493 mL; whereas, according to the same table, the decrease of distance (*x*) by 10 cm increases the total production by only 80 mL.

The theoretical variation of production as a function of thickness for different insulation materials on 13 March is illustrated in Fig. 9. The augmentation of thickness reduces the heat losses to solar still outside and, consequently, the production increases. The production increase

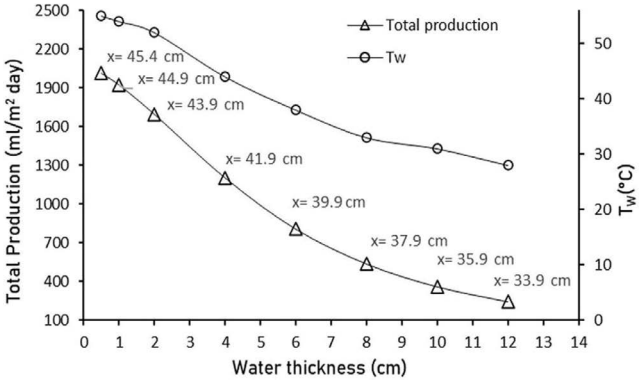

Fig. 8. Total production and saline water temperature at 1:00 pm vs. water thickness.

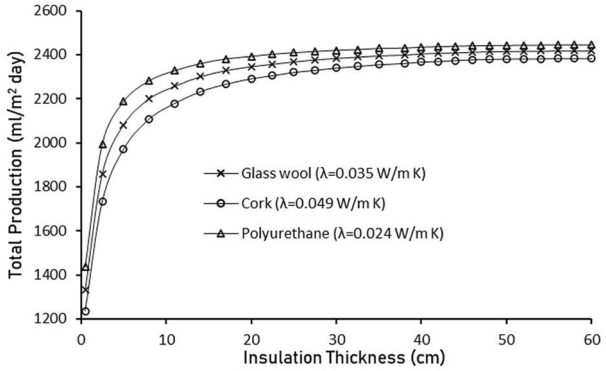

Fig. 9. Production vs. insulation thickness on 13 March.

is important at the beginning, gradually decreases with increased thickness, then tends to stabilize from a thickness close to 28 cm. Beyond this thickness, the increase in production is very low, which shows that we get closer to equilibrium. Thus, 28 cm can be chosen as the optimum thickness. Furthermore, it is noticeable that polyurethane ensures a higher production than other insulations for the same thickness because it has the lowest thermal conductivity. A 2.5-cm thick polyurethane insulation provides a production of 135 and 127 mL higher than that of glass wool and cork, respectively. The higher the insulation thickness is, the smaller the production margin between different insulations is.

6. Conclusion

This work presents the modeling of single-slope solar still based on energy and mass balances equations. The model results show a good match with the experimental ones. A parametric study was carried out to find the best distiller performance. Our findings show that production decreases when the solar still height increases for constant water depth, constant basin surface, and fixed tilt angle. Besides, the production is more important for condensation surfaces with high contact angle, such as glass. The maximal hourly distillate rate for glass is almost twice higher than that for plexiglass. Moreover, the increase of water depth for the same solar intensity reduces the water temperature, and therefore production decreases. The model results also show the effect of insulation type and thickness on solar still production. We found that the production rises with the increase of the insulation thickness and tends to stabilize beyond a thickness of 28 cm. The solar still production is 135 and 127 mL higher with polyurethane than glass wool and cork, respectively, for a thickness of 2.5 cm. The difference between the productions for different insulations becomes smaller with increased thickness.

Abbreviations

C_p	—	Specific heat, J/kg°C
g	—	Gravity acceleration, m/s^2
G	—	Solar intensity, W/m^2
Gr	—	Grashof number
Gr_m	—	Modified Grashof number
H, h	—	Heights, m
H_m	—	Average height, m
h	—	Heat coefficient, W/m^2 K
h_m	—	Convective mass transfer coefficient, m/s
K	—	Thermal conductivity, W/m K
Le	—	Lewis number
L_v	—	Latent heat of vaporization of water, J/kg
L	—	Thickness, m
m	—	Mass, kg
M	—	Molecular weight, kg/mol
$\dot{m}$	—	Distillate rate, kg/s
Nu	—	Nusselt number
P	—	Pressure, Pa
Pr	—	Prandtl number
q	—	Heat transfer, W/m^2
Ra	—	Rayleigh number
R	—	Universal gas constant, J/mol K
S	—	Area, m^2
T	—	Temperature, K
V	—	Cumulative production, mL/d
V_{wind}	—	Wind velocity, m/s
x	—	Distance between evaporation surface and condensation surface, m

Greek

α	—	Absorptivity
β	—	Volumetric thermal expansion coefficient, 1/K
ε	—	Emissivity
ε_{eff}	—	Effective emissivity
σ	—	Stefan–Boltzmann constant, W/m^2 K^4
ρ	—	Density, kg/m^3
τ	—	Transmittance
μ	—	Dynamic viscosity, Ns/m^2

Subscripts

a	—	Ambient air
b	—	Basin
c	—	Convection
dr	—	Droplets
e	—	Evaporation
ha	—	Humid air

i	—	Insulation
losses(b)	—	Losses from basin to distiller outside
Pg	—	Plexiglass
r	—	Radiation
ss	—	Still sides
w	—	Water

References

[1] S.W. Sharshir, G. Peng, L. Wu, N. Yang, F.A. Essa, A.H. Elsheikh, Showgi I.T. Mohamed, A.E. Kabeel, Enhancing the solar still performance using nanofluids and glass cover cooling: experimental study, Appl. Therm. Eng., 113 (2017) 684–693.

[2] A.E. Kabeel, Z.M. Omara, F.A. Essa, Numerical investigation of modified solar still using nanofluids and external condenser, J. Taiwan Inst. Chem. Eng., 75 (2017) 77–86.

[3] M.T. Chaichan, H.A. Kazem, Using aluminium powder with PCM (paraffin wax) to enhance single slope solar water distillation productivity in Baghdad–Iraq winter weathers, Int. J. Renewable Energy Res., 5 (2015) 251–257.

[4] A.E. Kabeel, S.A. El-Agouz, R. Sathyamurthy, T. Arunkumar, Augmenting the productivity of solar still using jute cloth knitted with sand heat energy storage, Desalination, 443 (2018) 122–129.

[5] H.N. Panchal, P. Shah, Effect of varying glass cover thickness on performance of solar still: in a winter climate conditions, Int. J. Renewable Energy Res., 1 (2012) 212–223.

[6] J. Xiong, G. Xie, H. Zheng, Experimental and numerical study on a new multi-effect solar still with enhanced condensation surface, Energy Convers. Manage., 73 (2013) 176–185.

[7] A. Abdessemed, C. Bougriou, D. Guerraiche, R. Abachi, Effects of tray shape of a multi-stage solar still coupled to a parabolic concentrating solar collector in Algeria, Renewable Energy, 132 (2019) 1134–1140.

[8] H.B. Halima, N. Frikha, R.B. Slama, Numerical investigation of a simple solar still coupled to a compression heat pump, Desalination, 337 (2014) 60–66.

[9] K. Hidouri, D.R. Mishra, A. Benhmidene, B. Chaouachi, Experimental and theoretical evaluation of a hybrid solar still integrated with an air compressor using ANN, Desal. Water Treat., 88 (2017) 52–59.

[10] M.M. Morad, H.A. El-Maghawry, K.I. Wasfy, Improving the double slope solar still performance by using flat-plate solar collector and cooling glass cover, Desalination, 373 (2015) 1–9.

[11] R.V. Dunkle, Solar Water Distillation: the Roof Type Still and a Multiple Effect Diffusion Still, Proceedings of the International Heat Transfer Conference, University of Colorado, USA, 1961, p. 895.

[12] M. Jakob, P.C. Gupta, The evaporation of liquid into a gas, Chem. Eng. Process, 50 (1954) 15.

[13] B.F. Sharpley, L.M.K. Boelter, Evaporation of water into quiet air from a one-foot diameter surface, Ind. Eng. Chem., 30 (1938) 1125–1131.

[14] K. Hidouri, S. Gabsi, Correlation for Lewis number for evaluation of mass flow rate for simple/hybrid solar still, Desal. Water Treat., 57 (2016) 6209–6216.

[15] P. Dumka, D.R. Mishra, Energy and exergy analysis of conventional and modified solar still integrated with sand bed earth: study of heat and mass transfer, Desalination, 437 (2018) 15–25.

[16] A.F. Mohamed, A.A. Hegazi, G.I. Sultan, E.M. El-Said, Augmented heat and mass transfer effect on performance of a solar still using porous absorber: experimental investigation and exergetic analysis, Appl. Therm. Eng., 150 (2019) 1206–1215.

[17] B. Jamil, N. Akhtar, Effect of specific height on the performance of a single slope solar still: an experimental study, Desalination, 414 (2017) 73–88.

[18] M.K. Phadatare, S.K. Verma, Effect of cover materials on heat and mass transfer coefficients in a plastic solar still, Desal. Water Treat., 2 (2009) 254–259.

[19] R. Bhardwaj, M. Ten Kortenaar, R. Mudde, Influence of condensation surface on solar distillation, Desalination, 326 (2013) 37–45.

[20] Z. Hongfei, Z. Xiaoyan, Z. Jing, W. Yuyuan, A group of improved heat and mass transfer correlations in solar stills, Energy Convers. Manage., 43 (2002) 2469–2478.

[21] H. Al-Hinai, M.S. Al-Nassri, B.A. Jubran, Parametric investigation of a double-effect solar still in comparison with a single-effect solar still, Desalination, 150 (2002) 75–83.

[22] H.Ş. Aybar, H. Assefi, Simulation of a solar still to investigate water depth and glass angle, Desal. Water Treat., 7 (2009) 35–40.

[23] M. Abu-Arabi, Y. Zurigat, H. Al-Hinai, S. Al-Hiddabi, Modeling and performance analysis of a solar desalination unit with double-glass cover cooling, Desalination, 143 (2002) 173–182.

[24] Y.H. Zurigat, M.K. Abu-Arabi, Modelling and performance analysis of a regenerative solar desalination unit, Appl. Therm. Eng., 24 (2004) 1061–1072.

[25] G. Menguy, M. Schwartz, Le Rayonnement Solaire Conversion Thermique et Application, Tec et Doc, Paris, 1980.

[26] A. Madhlopa, C. Johnstone, Numerical study of a passive solar still with separate condenser, Renewable Energy, 34 (2009) 1668–1677.

[27] O.O. Badran, M.M. Abu-Khader, Evaluating thermal performance of a single slope solar still, Heat Mass Trans., 43 (2007) 985–995.

[28] B.J. Briscoe, K.P. Galvin, The effect of surface fog on the transmittance of light, Solar Energy, 46 (1991) 191–197.

Supplementary information

Table S1 Quantitative comparison of theoretical and experimental production

28 February		Water depth = 1.6 cm		
t (h)	$V_{experimental}$ (mL)	$V_{theoretical}$ (mL)	Absolute error (mL)	Relative error (%)
9	0	0	0	–
10	0	10	10	–
11	0	74	74	–
12	170	176	6	3.53
13	260	275	15	5.77
14	351	320	31	–8.83
15	360	315	45	–12.5
16	280	267	13	–4.64
17	200	200	0	0
18	124	124	0	0
13 March		Water depth = 1.3 cm		
9	0	0	0	–
10	0	21	21	–
11	76	120	44	57.89
12	254	235	19	–7.48
13	348	304	44	–12.64
14	340	327	13	–3.82
15	300	305	5	1.67
16	240	251	11	4.58
17	174	183	9	5.17
18	120	114	6	–5
14 March		Water depth = 2.8 cm		
9	0	0	0	–
10	0	4	4	–
11	0	32	32	–
12	72	95	23	31.94
13	200	174	26	–13
14	270	234	36	–13.33
15	269	258	11	–4.09
16	220	245	25	11.36
17	188	212	24	12.77
18	148	160	12	8.11